Secular Trends in Global Tides derived from Satellite Radar Altimetry

I. Bij de Vaate[1], D. C. Slobbe[1], M. Verlaan[2,3]

[1]Civil Engineering and Geosciences, Delft University of Technology, Delft, The Netherlands
[2]Delft Institute of Applied Mathematics, Delft University of Technology, Delft, The Netherlands
[3]Deltares, Delft, Netherlands

Key Points:

- Satellite altimetry has for the first time been used to assess large scale secular trends in global tides
- Secular trends in the M_2, S_2, O_1, and K_1 tides are observed across the globe, with amplitude changes up to ±1 mm/year
- Global altimetry-derived trends have magnitudes and spatial variability comparable to estimates at tide gauges

Corresponding author: I. Bij de Vaate, `i.bijdevaate@tudelft.nl`

Abstract

Previous studies have demonstrated that tides are subject to considerable changes on secular time scales. However, these studies rely on sea level observations from tide gauges that are predominantly located in coastal and shelf regions and the large-scale patterns remain uncertain. Now, for the first time, satellite radar altimetry (TOPEX/Poseidon & Jason series) has been used to study worldwide linear trends in tidal harmonic constants of four major tides (M_2, S_2, O_1, and K_1). This study demonstrates both the potential and challenges of using satellite data for the quantification of such long-term changes. Two alternative methods were implemented. For the first method, tidal harmonic constants were estimated for consecutive four year periods, from which the linear change was then estimated. For the second method, the estimation of linear trends in the tidal constants of the four tides was integrated in the harmonic analysis. First, both methods were assessed by application to tide gauge data that were sub-sampled to the sampling scheme of the satellites. Thereafter the methods were applied to the real satellite data. Results show both statistically significant decreases and increases in amplitude up to 1 mm/year and significant phase changes up to $\sim$0.1 deg/year. Overall, altimeter-derived trends agree with estimates from tide gauge data, while contradictions are observed in some locations. However, direct comparisons with tide gauges should be treated carefully.

Plain Language Summary

Tidal predictions are valuable for many purposes, ranging from processing satellite data to coastal engineering. Although tidal constants are often perceived to be stationary in time, earlier studies have shown that tides are subject to changes both on seasonal and long-term time scales. However, these studies mainly concern coastal data and therefore, the processes at open ocean remain unclear. The study behind this paper is the first that uses global satellite data to quantify secular trends in tides, thereby filling in the gaps of earlier work. Results show the changes in tides to be significant, with both decreases and increases in tidal amplitude of the order of several centimeters and phase changes of several degrees over the past decades.

1 Introduction

Knowledge of tides is important for many practical (e.g., marine navigation, fishery, coastal engineering) and scientific purposes. Although tide predictions often treat tidal harmonic constants as stationary over time, considerable changes in tides have been observed on seasonal (e.g., Bij de Vaate et al., 2021; Müller et al., 2014) to long-term timescales (e.g., Müller et al., 2011; Ray, 2016). On the one hand, modifications of the tides can be the result of local processes, such as changes in coastal morphology or altered river flow (Haigh et al., 2020). On the other hand, observed variations in tides have been linked to regional climatic conditions, e.g., the extent of sea ice coverage (e.g., Bij de Vaate et al., 2021; Müller et al., 2014; St-Laurent et al., 2008), ocean stratification (e.g., Müller, 2012; Müller et al., 2014), and sea level rise (e.g., Devlin et al., 2017; Ross et al., 2017). Modelling studies suggest that climate change will continue to affect tides for centuries (Pickering et al., 2017; Schindelegger et al., 2018). Nevertheless, Haigh et al. (2020) indicated the need for better understanding of individual contributions of small-scale and large-scale processes.

An increasing number of studies are devoted to mapping and understanding secular changes in the tides. However, most of these studies rely on sea level observations from tide gauges that are mainly restricted to coastal and shelf regions. Hence, observed changes in tides are likely dominated by local processes and the large-scale patterns remain unclear. Obtaining the global picture of long-term changes in tides would contribute to a better understanding of the drivers behind secular changes in tides. Understanding secular changes in tides may result in better identification and prediction of any consequences for coastal environments such as flooding (Li et al., 2021), salt intrusion (Hinton, 2000), or altered estuarine dynamics (Khojasteh et al., 2021).

To gain more insight in the large-scale secular changes in tides, we supplemented the clustered and sparsely distributed tide gauge dataset by data from satellite radar altimeters. Altimeter-derived water levels are being widely used to estimate tidal constants, and have recently been used to study seasonal changes in tides (Bij de Vaate et al., 2021; Müller et al., 2014). However, up to now, only Ray (2016) used altimeter data from successive missions to compare the amplitude of the main semi-diurnal tide (M_2) near Churchill, Hudson Bay (Canada). Given the length of the current satellite altimeter records ($>$ 25 years), from a theoretical point of view it should be possible to obtain estimates of the secular changes in tides from these data. For that reason, we have exploited the provided opportunities and used data from TOPEX/Poseidon and the Jason satellites to obtain a global estimate of the linear secular trends in the major tides. In this paper we first describe the data, including satellite radar altimetry, high-frequency tide gauge records and reanalysis data used for validation of the results. Then an outline is given of two approaches to study secular changes in tides and an experiment to test these methods. Finally, the results are introduced and compared to observations at tide gauges and documented changes in tides.

2 Data

2.1 Satellite Radar Altimetry

Data from the TOPEX/Poseidon and Jason satellite altimeters were combined (further referred to as TPJ) resulting in 28 years of sea level data (1993-2020). Data from interleaved orbits were not considered. The TPJ satellites have a ground coverage up to 66°N/S and an along-track resolution of about 5.8 km. Altimeter data were obtained through the Radar Altimeter Data System (RADS, `http://rads.tudelft.nl/rads/rads.shtml`). The following geophysical and range corrections were applied (Scharroo et al., 2016): ionosphere (NIC09 for TOPEX/Poseidon, GIM for Jason), dry troposphere (ECMWF), wet troposphere (if available: radiometer, otherwise: ECMWF), solid tide (Cartwright & Edden, 1973; Cartwright & Taylor, 1971), pole tide (Wahr, 1985), load tide (FES2014), mean sea surface (DTU18-MSS), sea state bias (CLS), and dynamic atmosphere (DAC) (MOG2d (ERA Interim forcing)). The center-of-gravity (CG) correction that RADS by default applies to TOPEX/Poseidon ranges was removed to reduce intermission biases in the solar S_2 tide (Beckley et al., 2021; Zawadzki et al., 2018). In addition, to minimize aliasing of non-tidal sea level variability on tidal frequencies, an additional correction was applied. Following Ray and Zaron (2016), the multi-mission, gridded sea level anomalies (SLA) from the Data Unification and Altimeter Combination System (DUACS) (Taburet et al., 2019) were subtracted from the TPJ-water levels. This removes seasonal and interannual variability from the obtained water levels and specifically reduces the noise in regions with high mesoscale activity. In the remainder of the paper, this correction will be referred to as the 'mesoscale correction'. Finally, outliers in the time series were detected and removed based on three times the median absolute deviation.

In this paper, results are presented on global maps, supplemented by a zoom in on the North West European Shelf. For the global analysis data are treated as follows. First, the locations where two tracks intersect (crossovers) were identified. For all of those locations, the data of the two crossing tracks within a radius of 30 km were assigned to the location of the respective crossover. 30 km equals half the distance between the closest neighbouring crossovers. Note that the along-track distance between crossovers depends on latitude: from $\sim$460 km at the equator to $\sim$60 km at 66°N/S. By stacking the data at crossover locations, the temporal resolution is increased and tidal analysis is deemed more reliable. For the zoom in on the North West European Shelf, data were processed on a track-by-track basis. Data from different cycles were collocated following Cherniawsky et al. (2010). The along-track analysis allows for a higher spatial resolution and to get closer to the tide gauge locations, at the price of an increase in uncertainty levels.

2.2 Tide Gauges

Alongside the altimeter data, data from a selection of tide gauges were processed to allow for a comparison of the derived trends. For this purpose, only tide gauge data from the TPJ-period were considered (1993-2020). Data from the GESLA-3 dataset (Haigh et al., 2021) were complemented with quality controlled water level records from tide gauges on the North West European Shelf, provided by nine European organizations (see Acknowledgments). The latter comprise data from 1997 onwards, and are manually inspected to exclude possible outliers. Records that span less than 19 years were excluded. The temporal resolution of the tide gauge data varies from one minute to one hour, mainly depending on the country where the stations are located and the time of data acquisition. Tide gauge records were corrected for atmospheric loading using the same product as was used for altimetry (DAC).

2.3 Reanalysis Data

Finally, reanalysis data were used to obtain uncertainty estimates of the estimated linear change in tidal constants. For this, the Global Tides and Surge Model (GTSM, Wang et al., 2021) was used, forced by ERA5 reanalysis data. GTSM is a barotropic (2D) model that makes use of an unstructured grid with a resolution that increases from 25 km at open ocean to 2.5 km at the coast. Time series with a sampling rate of 10 minutes were reconstructed for the full TPJ-period. This was done for over 600 locations covering the global oceans and about 300 locations on the western North West European Shelf. Subsequently, the model time series were corrected for atmospheric loading (using the DAC), temporarily detided and then subjected to a high-pass filter to remove any non-tidal signal with periods larger than 2 days. This was done to mimic the 'mesoscale correction' that was applied to the TPJ-data. Although the GTSM does not resolve ocean circulation and associated mesoscale sea level variability, atmospheric forcing may induce seasonal/interannual sea level variability (e.g., Dangendorf et al., 2014), which is to some extent also contained in the 'mesoscale correction'.

3 Methods

Earlier studies on secular changes in tides typically relied on year-by-year harmonic analyses of high-frequency data, followed by the fitting of a linear trend through the yearly tidal harmonic constants (e.g., Ray, 2009; Müller et al., 2011; Zaron & Ray, 2018). In this paper, a similar procedure was adopted to process the tide gauge data. However, for satellite data, such a procedure is not possible due to the relatively low sampling rate and consequent aliasing of high-frequency tidal signals onto lower frequencies. That is, for the major tides the TPJ-sampling interval of 9.9156 days results in alias periods of 62.1 (M_2), 58.7 (S_2), 173.2 (K_1), and 45.7 days (O_1) (Cherniawsky et al., 2010; Schrama & Ray, 1994). By applying the Rayleigh criterion to these alias frequencies, we can find the minimum record length that is required to separate the tides of interest from other signals (Savcenko & Bosch, 2007). For M_2, S_2, and O_1, records of three (2.97) years are sufficient to separate them from other considered constituents, while at least 9.19 years are required to separate K_1 from S_{sa} (semi-annual tide). Hence, a year-by-year harmonic analysis of TPJ-data is not possible. In this paper, two different methods were implemented.

Both approaches make use of UTide (Codiga, 2020). This software executes a harmonic analysis for a given set of frequencies similar as in TTide (Pawlowicz et al., 2002), yet it is able to deal with irregular temporal sampling. The latter is a requirement for processing stacked altimeter-derived water levels. For the analysis of tide gauge data a large set of constituents (including shallow water constituents), was considered following from the automated constituent selection method in UTide (Codiga, 2020; Foreman, 2004). For satellite data, a fixed set of constituents was considered, as explained below.

3.1 Segmented Harmonic Analysis (SegHA)

The first approach, referred to as the 'segmented harmonic analysis' (SegHA) approach (inspired by (Jin et al., 2018)), is a two-step procedure that is very similar to the conventional analysis of secular changes using tide gauge data. This approach could be carried out with standard tidal analysis tools, but comes at the price of a slight simplification in error propagation.

3.1.1 Step 1: Estimation of Tidal Harmonic Constants

Instead of processing the data year-by-year, time series were split in seven consecutive periods of four years. Thereafter, tidal harmonic constants were calculated and referred to the center date of the respective four-year period. The time span of four years was chosen primarily because this allows the separation of M_2, S_2, and O_1 from other signals (this requires at least 3 years). On the other hand, there is in some instances (mainly coastal) a discrepancy between the actual nodal modulation of lunar tides (18.6 year cycle) and the theoretical value (Hagen et al., 2021). Hence, although amplitude/phase estimates are corrected for the nodal modulation during tidal analysis, there may be a residual modulation left. To separate the trend in tidal amplitude from this possible residual of the nodal cycle, the difference between the respective center data of the first and last period was required to be at least 18.6 years. This can be achieved by processing segments of up to five years (segments are not allowed to overlap). Hence it is anyway not possible to study the secular trend in K_1 harmonic constants from the available data using the SegHA approach. Given the minimum of three years and the maximum of five years, a time span of four years was chosen since this allows making full use of the available data (28 years).

For each four-year period, tidal amplitudes and phases were estimated for 20 tidal constituents, including: three long-period tides (S_a, M_m, and M_{sf}), five diurnal tides (Q_1, O_1, P_1, S_1, and K_1), eight semi-diurnal tides ($2N_2$, μ_2, N_2, ν_2, M_2, L_2, T_2, S_2, and $2SM_2$), and four shorter period tides (M_3, MN_4, M_4, and MS_4). This selection of constituents eliminates possible conflicts between constituents pairs that cannot be separated from four years of data (e.g., K_1 and S_{sa}). In addition, from each four-year period the mean sea level (Z_0) and a possible trend in mean sea level were estimated to account for any remaining interannual sea level variability.

95% confidence intervals for the estimated harmonic constants were computed with UTide. This measure is derived from linearized error propagation of the total residual power (using the detided signal) within the frequency band surrounding the frequency in question ($M_2/S_2 \pm 0.2$ cycles/day and $O_1 \pm 0.1$ cycles/day), obtained using the Lomb-Scargle periodogram (Codiga, 2011; Pawlowicz et al., 2002). However, it is stated by Codiga (2011) that certain assumptions underlying this procedure are strictly valid only for uniformly sampled data. The resulting confidence intervals "should be considered potentially reasonable and approximate first estimates, but should be compared against the results for uniform times whenever possible, and used with a measure of caution." (Codiga, 2011, p. 21). Moreover, UTide averages the spectral density distribution of the residuals over nine frequency bands resulting in similar confidence intervals for all diurnal tides, all semi-diurnal tides, and so on. On the contrary, it was found that both the timing of the sea level measurements by the satellite and the frequency and amplitude of the non-tidal variations with respect to that of the tide in question, influenced the accuracy of the resulting tidal estimates (Guarneri et al., 2022). In line with the advice from Codiga (2011), but due to the lack of tide gauge data in the vicinity of the altimeter points, we have therefore obtained an additional (alternative) uncertainty estimate using the reanalysis data as described in Sect. 2.3 Reanalysis Data. These time series were reduced to a four year period (2015-2018) and interpolated to the TPJ-sampling interval of which the start time was iteratively shifted by about 4.75 hours (TPJ-sampling period divided by 50), resulting in 50 time-shifted time series. From these time series tidal harmonic constants were computed and compared to the actual values (derived from the original high-frequency time series). The mean absolute deviation between each of the 50 estimates and the actual value of the harmonic constant was perceived as the standard error of the estimate. The final values are location- and tide specific, but assumed to be independent of the four-year period.

3.1.2 Step 2: Linear Trend Estimation

The linear secular trends in harmonic constants were estimated by fitting the following equations through the series of seven values, using weighted least squares. Here noise correlations between amplitudes and phases are ignored. For amplitudes follows:

$$\tilde{A}_k(t_i) = \underbrace{a_k^{\mathrm{n}} \cos\left(2\pi \frac{t_i - t_c}{18.6} + N_c\right)}_{\text{residual nodal modulation}} + \underbrace{b_k^A (t_i - t_c)}_{\text{trend}}. \tag{1}$$

where, $\tilde{A}_k(t_i)$ is the residual amplitude for the ith four-year period of the tidal constituent in question (k) (obtained by subtracting the time averaged amplitude), b_k^A the linear change in amplitude, t_i the center time of the ith four-year periods, and t_c the center time of the full TPJ-period. In addition, the nodal modulation was included in the problem formulation (see Sect. 3.1.1 Step 1: Estimation of Tidal Harmonic Constants). N_c represents the nodal phase at the center date. Both the magnitude of the residual nodal modulation (a_k^{n}), and the linear amplitude change (b_k^A) were estimated, resulting in a redundancy of five. For the phases the following equation was used:

$$\tilde{\phi}_k(t_i) = \underbrace{a_k^{\mathrm{n}} \cos\left(2\pi \frac{t_i - t_c}{18.6} + N_c\right)}_{\text{residual nodal modulation}} + \underbrace{b_k^{\phi} (t_i - t_c)}_{\text{trend}}. \tag{2}$$

Where $\tilde{\phi}_k(t_i)$ is the residual phase for the ith four-year period, a_k^{n} the magnitude of the residual nodal phase modulation, and b_k^{ϕ} the linear coefficient describing the change in phase.

Both the standard errors of the harmonic constants derived from UTide and from GTSM (3.1.1 Step 1: Estimation of Tidal Harmonic Constants) were used to assess the significance of the fitted trends. For the S_2 tide, the choice of ionospheric correction applied to the data may affect the estimated tidal harmonic constants (Zawadzki et al., 2018). Therefore, an additional error estimate was obtained (see Text S1) and added to the estimates obtained by UTide and GTSM respectively. Given the standard errors of the tidal harmonic constants, the standard error of the trend was derived through error propagation. 95% confidence intervals were obtained by multiplying the standard error with 1.96.

3.2 Trend-integrated Harmonic Analysis (TintHA)

In the second approach, the linear trends in the four tides of interest (M_2, S_2, O_1, and K_1) were estimated jointly with the average tidal harmonic constants. This required an extension of the available tidal analysis software but allowed for a full error propagation (i.e., without ignoring covariances between trends in amplitudes and phases). Since we are now using the full 28 years of data, this approach allows the analysis of changes in the K_1 tide. Moreover, the set of constituents included in the analysis was extended by S_{SA}, K_2 and T_2. In the SegHA approach, these had to be excluded due to aliasing issues.

The TintHA approach uses a different formulation of the tides. Within UTide, the complex formulation is used in which the tidal water level for constituent k, i.e. $\hat{h}_k(t)$, is written as the product of three terms:

$$\hat{h}_k(t) = \left(A_k e^{i\phi_k}\right)\left(f_k(t)e^{iu_k(t)}\right)e^{iv_k(t)}, \tag{3}$$

where the term $e^{iv_k(t)}$ is the phase of the equilibrium tide, $\left(f_k(t)e^{iu_k(t)}\right)$ is the nodal correction, and the term $\left(A_k e^{i\phi_k}\right)$ is the complex amplitude-phase pair that needs to be estimated. To keep the equations linear, we consider the complex amplitude-phase pair $\hat{A}_k = A_k e^{i\phi_k}$:

$$\hat{A}_k(t) = \hat{F}_k + \hat{G}_k \frac{t - t_0}{T}, \tag{4}$$

where the time period considered starts at t_0 and ends at $t_0 + T$, so that $\hat{A}_k(t_0) = \hat{F}_k$ and $\hat{A}_k(t_0 + T) = \hat{F}_k + \hat{G}_k$. The relative change over this time period is $\hat{\Delta} = (\hat{F}_k + \hat{G}_k)/\hat{F}_k$. The angle and absolute value of this complex number give the phase change and relative amplitude change. A disadvantage of this linear model is that the rate of change of the amplitude and phase is not constant over the time interval. For small changes, however, the differences will be small. Note that in this method no empirically estimated correction for any residual of the nodal modulation is determined as this, in combination with the trend estimation, would result in a non-linear estimation problem.

Similar to the first approach (SegHA), alternative error estimates were obtained by means of the GTSM reanalysis data. For the latter, the full 28 year time series were used, although a linear trend in both amplitude and phase of M_2, S_2, O_1 and K_1 was manually imposed (1 mm/year for amplitude and 0.1 deg/year for phase). The time series were again interpolated to TPJ-sampling intervals while iteratively shifting the start time 50 times. From these time series the linear change in tidal harmonic constants was computed and compared to the imposed values. The mean absolute deviation between both products was perceived as the standard error of the trend estimates. For the S_2 tide, the error estimates were again supplemented by the possibly error due to the ionospheric correction (as described in Text S1). Final 95% confidence intervals were obtained by multiplying the error estimate by 1.96 and interpolating the GTSM-derived product to the TPJ-tracks.

3.3 Comparison of SegHA and TintHA using Tide Gauge Data

Both approaches (SegHA and TintHA) were tested by application to tide gauge data that were sub-sampled to TPJ-sampling intervals (both considering an along-track sampling of 9.9156 days and a crossover sampling which is assumed to be half of 9.9156 days), while randomly shifting the starting time. For each tide gauge, 10 time series were generated. For this assessment, only tide gauges were considered that have full data coverage during the entire TPJ-period. In addition to DAC, the 'mesoscale correction' was applied to the data to mimic the processing of altimeter data. As this altimetry-derived product is not available everywhere across the globe, data from only 45 tide gauges could be used. The secular change in tidal harmonic constants derived from both methods was compared to the 'true' change as obtained by processing the original high-frequency data on a year-by-year basis. This assessment was done by computing the median absolute deviation (MAD) for respectively each tide gauge, tidal constituent and method.

3.4 Post-processing

Estimated trends were omitted for locations where at least one of the following criteria was not met. If not mentioned otherwise, these criteria were applied in the analysis of the crossovers, individual tracks, and tide gauges:

- The root-mean-square deviation (RMS) of the residual signal should be below 0.15 m. Globally, this removes $\sim 8\%$ of the data.
- There should be sufficient data coverage for all four year periods. A location was not considered when during any of the respective periods more than 10 sequential calendar days have no data. Globally, this removes $\sim 20\%$ of the data.

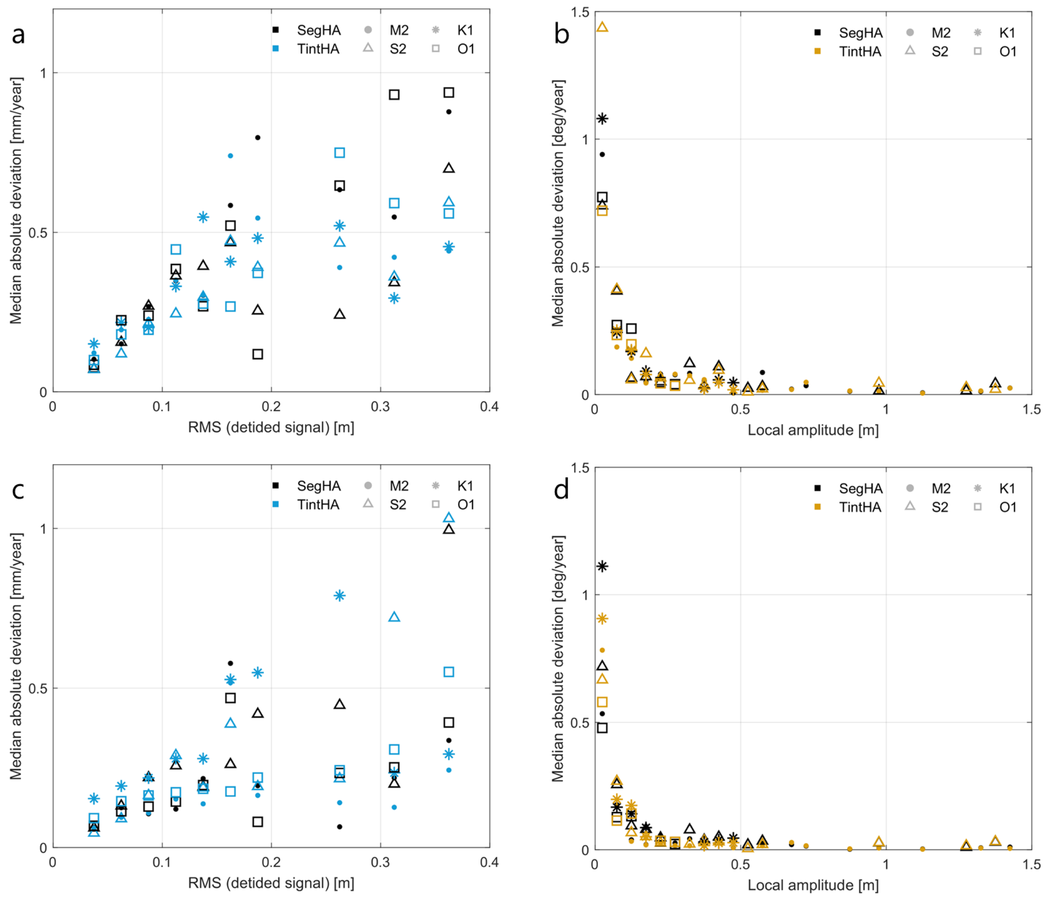

Figure 1: Median absolute deviation between the 'true' linear change in amplitudes (a, c) and phases (b, d) derived from high-frequency tide gauge records and the product derived from the SegHA and TintHA approaches applied to the data sub-sampled at TPJ along-track sampling intervals (a, b) and TPJ crossover sampling (c, d). Colours indicate which method was used and the marker style depicts the different tidal constituents that were studied. For visualisation purposes the deviations are averaged for intervals of 0.025 m and 0.05 m for the RMS (detided signal) and local amplitude respectively.

- The estimated linear coefficient should be larger than its 95% confidence interval. Which confidence intervals were used (UTide- vs. GTSM-based) is mentioned in figure captions.
- Only applied in along-track analysis: crossovers where there is no overlap between the estimated linear trends of the two crossing tracks (interpolated to the location of the crossover) ± the local confidence interval, were flagged. In such a case, all derived trends of the two crossing tracks within half the distance between neighbouring crossovers were omitted.

4 Results

4.1 Comparison of SegHA and TintHA using Tide Gauge Data

Comparison of both methods applied to tide gauge data shows little difference between the SegHA and TintHA methods (Figure 1). Despite the method that is used, sub-sampling

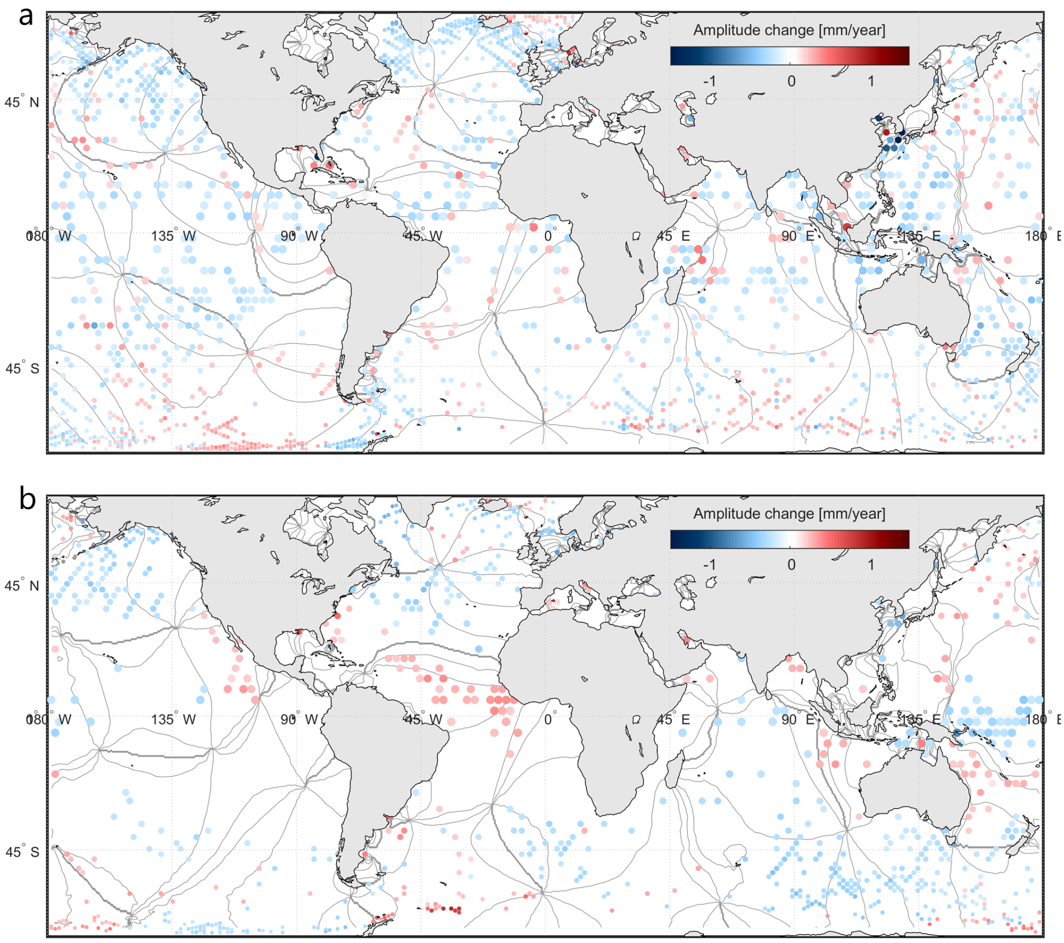

Figure 2: Linear change in M_2 (a) and S_2 amplitude (b) per year (1993-2020) following the TintHA approach. Scatter size reduces with latitude to reduce cluttering at high latitudes. Locations where the post-processing criteria (including both UTide- and GTSM-derived 95% confidence intervals) were not met are excluded from the figure. Lines in the background depict tidal phases at 45° intervals.

the data to TPJ-sampling interval reduces the accuracy of the derived changes in tidal amplitude and phase. In the case of amplitude, the observed deviation between the 'true' and derived change increases with larger non-tidal water level variation (higher RMS; Figure 1a). On the other hand, the accuracy of the derived phase change predominantly depends on the local amplitude of the tide in question (Figure 1b). In particular for amplitudes below ~ 15 *cm* the derived phase change appears unreliable. Only in terms of amplitude change, the TintHA method performs more consistent than the SegHA method, with an average MAD of 0.22 mm/year compared to 0.25 mm/year and fewer outliers. Overall, the crossover sampling improves the accuracy of both methods for both amplitudes (average deviation reduces from 0.23 mm/year to 0.14 mm/year) and phases (0.31 °/year to 0.23 °/year) for all tides except K_1 (Figure 1c, d).

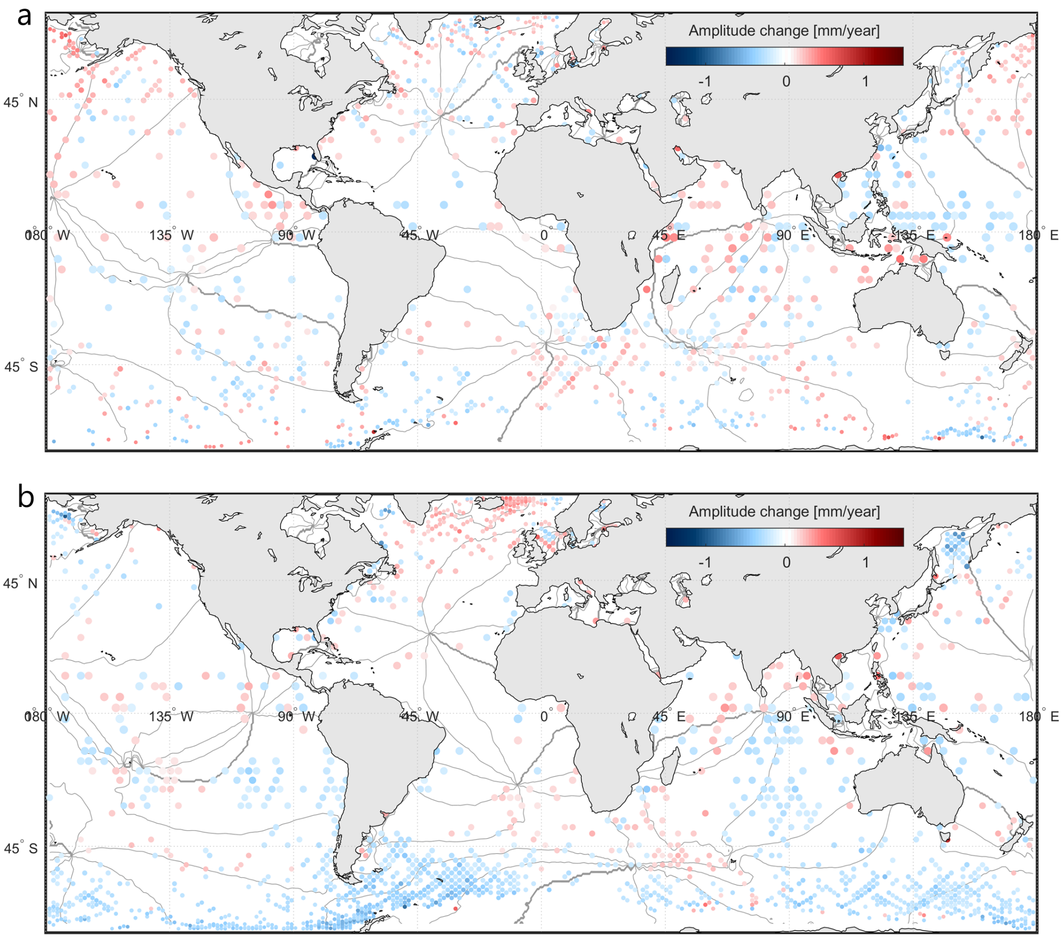

Figure 3: Linear change in O_1 (a) and K_1 amplitude (b) per year (1993-2020) following the TintHA approach. Scatter size reduces with latitude to reduce cluttering at high latitudes. Locations where the post-processing criteria (including both UTide- and GTSM-derived 95% confidence intervals) were not met are excluded from the figure. Lines in the background depict tidal phases at 45° intervals.

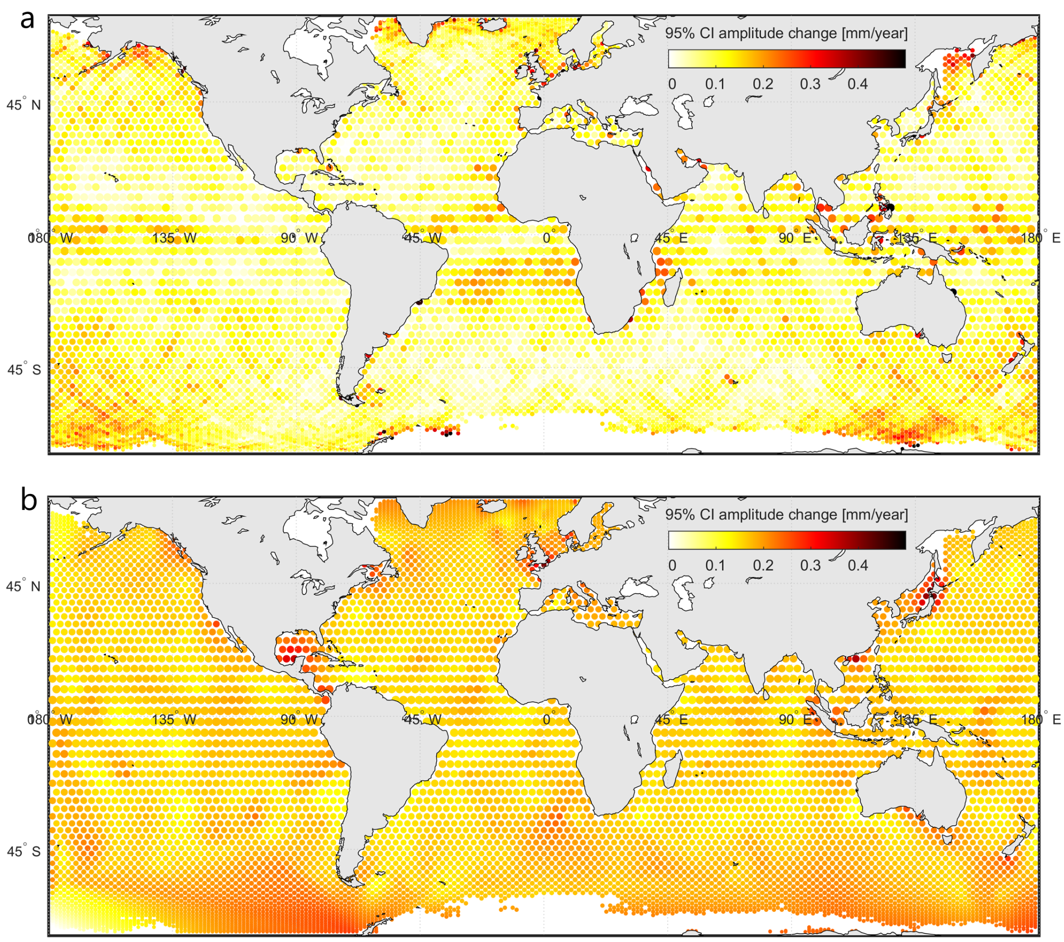

Figure 4: 95% confidence intervals for trend estimates derived from confidence intervals computed by UTide (a) and from standard errors derived from GTSM (b) for M_2 amplitude.

4.2 Global Analysis

The estimated trends in amplitude at the TPJ-crossovers following from the TintHA approach, are displayed in Figures 2 and 3. The results produced by the SegHA method are very similar and incorporated in the Supporting Information (Figure S6). Clearly, regions that are covered by sea ice during part of the year (above 55°N/S), have insufficient data availability for this analysis and are excluded. The distribution of locations where the estimated trend coefficients are significant, varies per tidal constituent, which is closely related to the confidence intervals (Figures 4, S2 and S3). Here, the GTSM-derived confidence intervals (e.g., Figure 4b) are in most locations larger than the intervals derived by UTide (Figure 4a).

As can be seen in Figure 2 and 3, all tides are subject to yearly changes of up to ±1 mm/year. The magnitude and sign of the yearly change vary largely across the globe, while the spatial correlations of the signal vary per tide. For M_2, the change in amplitude is predominantly negative. The most obvious regions of positive change are in the south, near Antarctica and east of Iceland (Figure 2a). Although the overall change is rather heterogeneous, spatial correlation of the signal is stronger near the poles than at the lower latitudes. On the contrary, the change in S_2 amplitude shows more distinct regions of either positive or negative change across the globe (Figure 2b). Predominantly positive changes in amplitudes are observed around the equator and near the poles, while negative changes are more restricted to mid-latitudes. Differences in sign of the amplitude change appear closely related to the location of amphidromic points and co-phase lines. The change in O_1 amplitude is more similar to that of M_2, concerning the level of heterogeneity and the predominant change being negative (Figure 3a). However, near the equator, the average change in O_1 amplitude is smaller than that of M_2. Moreover, where the M_2 amplitudes show a decline in the Gulf of Alaska, O_1 amplitudes mainly increase in this region. For K_1 predominant negative changes are observed across the globe, except for the north Atlantic and the Indian Ocean (Figure 3b).

Trend estimates derived from the global tide gauge dataset are shown in Figures 5 and 6. Where possible, derived trends at TPJ-crossovers were compared to trends derived from nearby tide gauges (see Text S2). For M_2 and S_2 69% of the differences in trend estimates from tide gauges and TPJ-crossovers was statistically insignificant (i.e., difference $< 2 * \mathrm{SE}_{\mathrm{trend}}$, where $\mathrm{SE}_{\mathrm{trend}}$ is the standard error of the trend estimate, derived from GTSM. For O_1 and K_1 63% of the differences were insignificant. However, note that this measure takes into account the expected spatial variability. Given the distance between TPJ-crossovers and most tide gauges being at least 50 km (Figure S1b), in particular the expected spatial variability in M_2 trend estimates is significant (Figure S1a).

4.3 North West European Shelf

A selection of results from the along-track analysis of the North West European Shelf region is displayed in Figure 7. Because of their relatively low amplitudes in the region (< 0.15 m), O_1 and K_1 are not included here.

The M_2 amplitude change derived from altimetry is predominantly negative, except for a few regions: the central North Sea, the southwest corner of the domain, and some small areas around Norway (Figure 7a). The largest change is observed in the North Sea. Unfortunately most of the tide gauges are located along the coastline while RADS does not include coastal altimeter data. Nevertheless, the observed amplitude change at the tide gauges in the Netherlands, Germany, Denmark (and to a smaller extent the United Kingdom and Norway), is similar to that at nearby tracks. Limited similarity is observed for the tide gauges surrounding the English Channel and the Irish sea. However, as can be seen in Figure 7e, the distance between the majority of the tide gauges and the nearest TPJ-track is 30 km at minimum. It can also be seen that the overall similarity between tide gauges and the nearest track reduces increases when the TPJ-track is located in deeper water. When the track covers shallow water, the differences are significantly larger. The altimetry-derived change in M_2 phase is largest near the amphidromic points in the North Sea and in the northwest corner of the region (Figure 7c). Overall, both the sign of the phase change as derived from altimetry as well as from tide gauges, is highly variable within the domain. In addition, the availability of significant altimetry-derived phase changes near tide gauges is even more limited than was the case for the amplitude, making a comparison difficult. The observed trends in S_2 amplitude are smaller than those in M_2 amplitude (Figure 7b), while the change in phase is larger (Figure 7d). These differences in magnitude are also observed at the tide gauges.

Both GTSM and UTide-derived confidence intervals increase towards the coast for the amplitude change (Figure 8a, 8b, 9a and 9b) and towards amphidromic points for the phase change (Figure 8c, 8d, 9c and 9d). In all cases, the GTSM-derived confidence intervals exceed the ones computed by UTide. This is most noticeable for the S_2 amplitude change. Both GTSM- and UTide-derived confidence intervals for S_2 phase change are significantly larger than for M_2.

5 Discussion and Conclusions

Using the full record of sea level measurements by the TOPEX/Poseidon and Jason satellites (1993–2020), a global estimate of the secular trends in M_2, S_2, O_1, and K_1 tidal

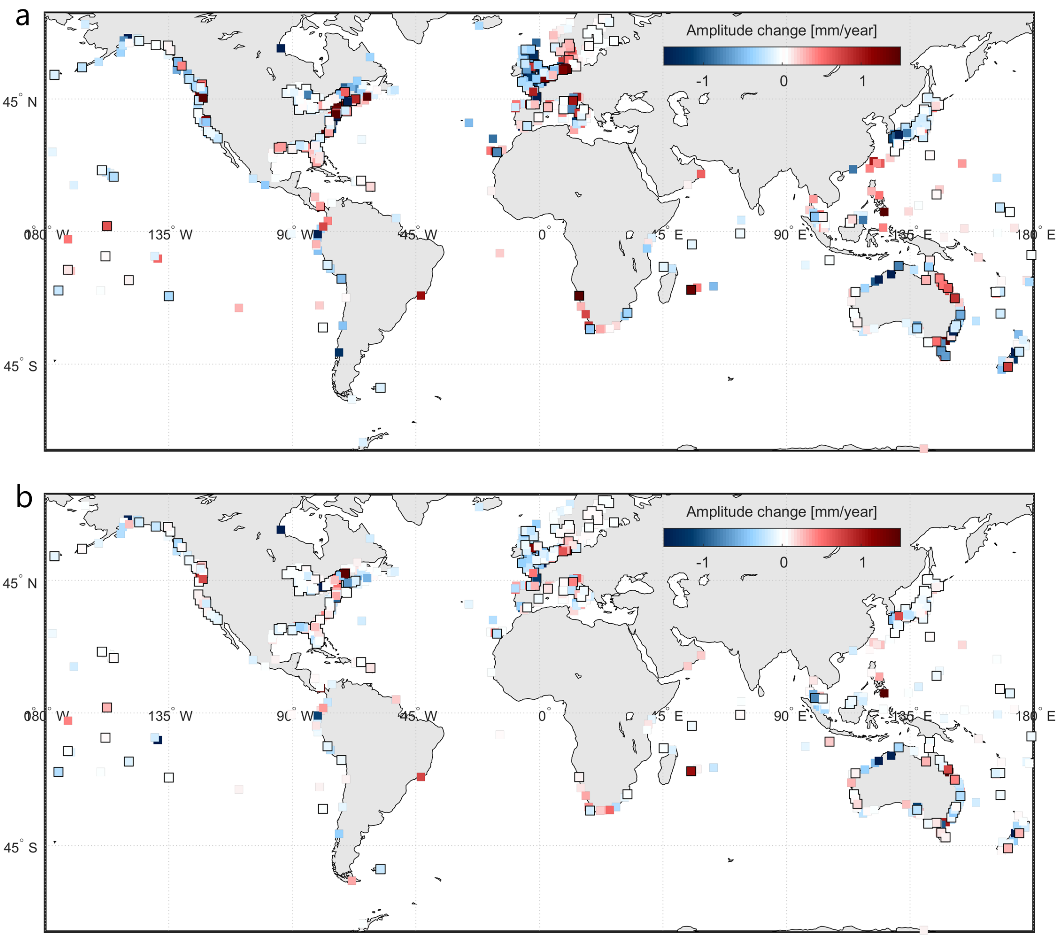

Figure 5: Secular trends in M_2 (a) and S_2 (b) amplitudes, derived from tide gauge records from the TPJ-period (1993-2020) (from GESLA-3; Haigh et al. (2021)). Black-outlined tide gauge locations are within 75 km of a TPJ-crossover and are used for the similarity measure as explained in text S2.

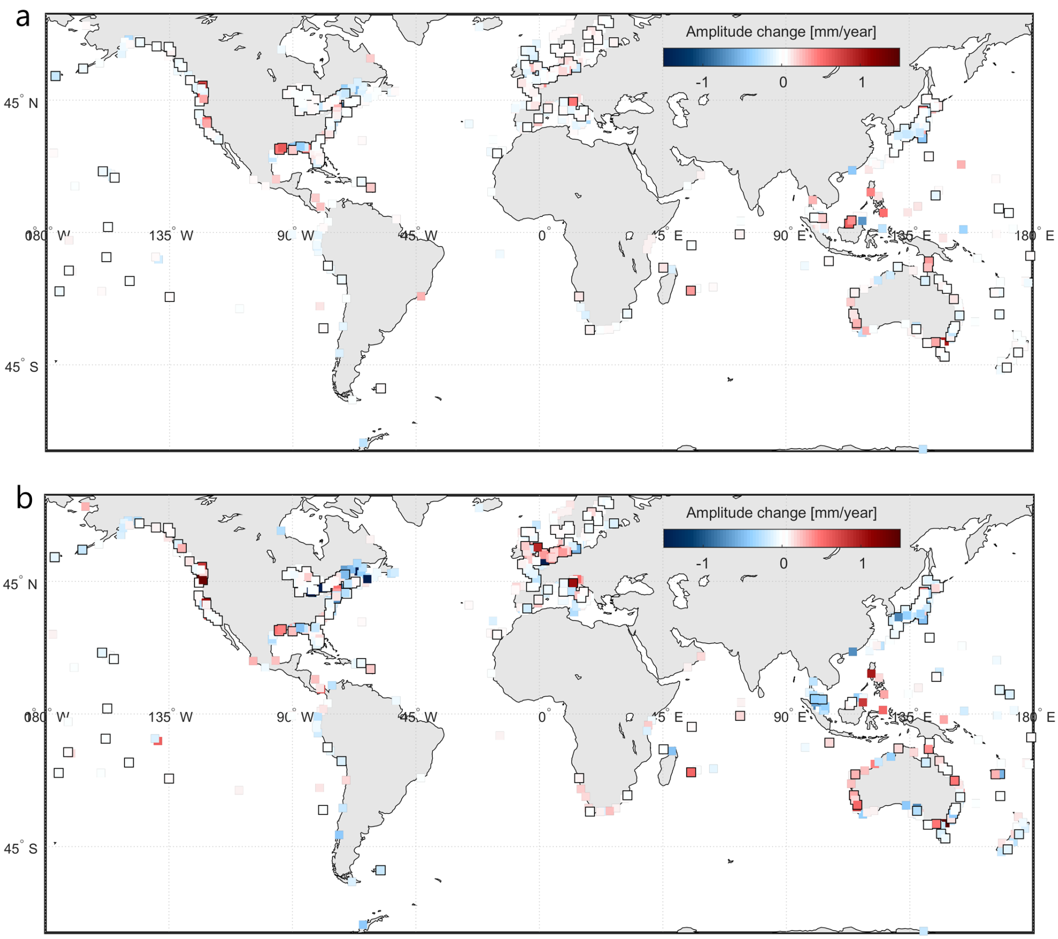

Figure 6: Secular trends in O_1 (a) and K_1 (b) amplitudes, derived from tide gauge records from the TPJ-period (1993-2020) (from GESLA-3; Haigh et al. (2021)). Black-outlined tide gauge locations are within 75 km of a TPJ-crossover and are used for the similarity measure as explained in text S2.

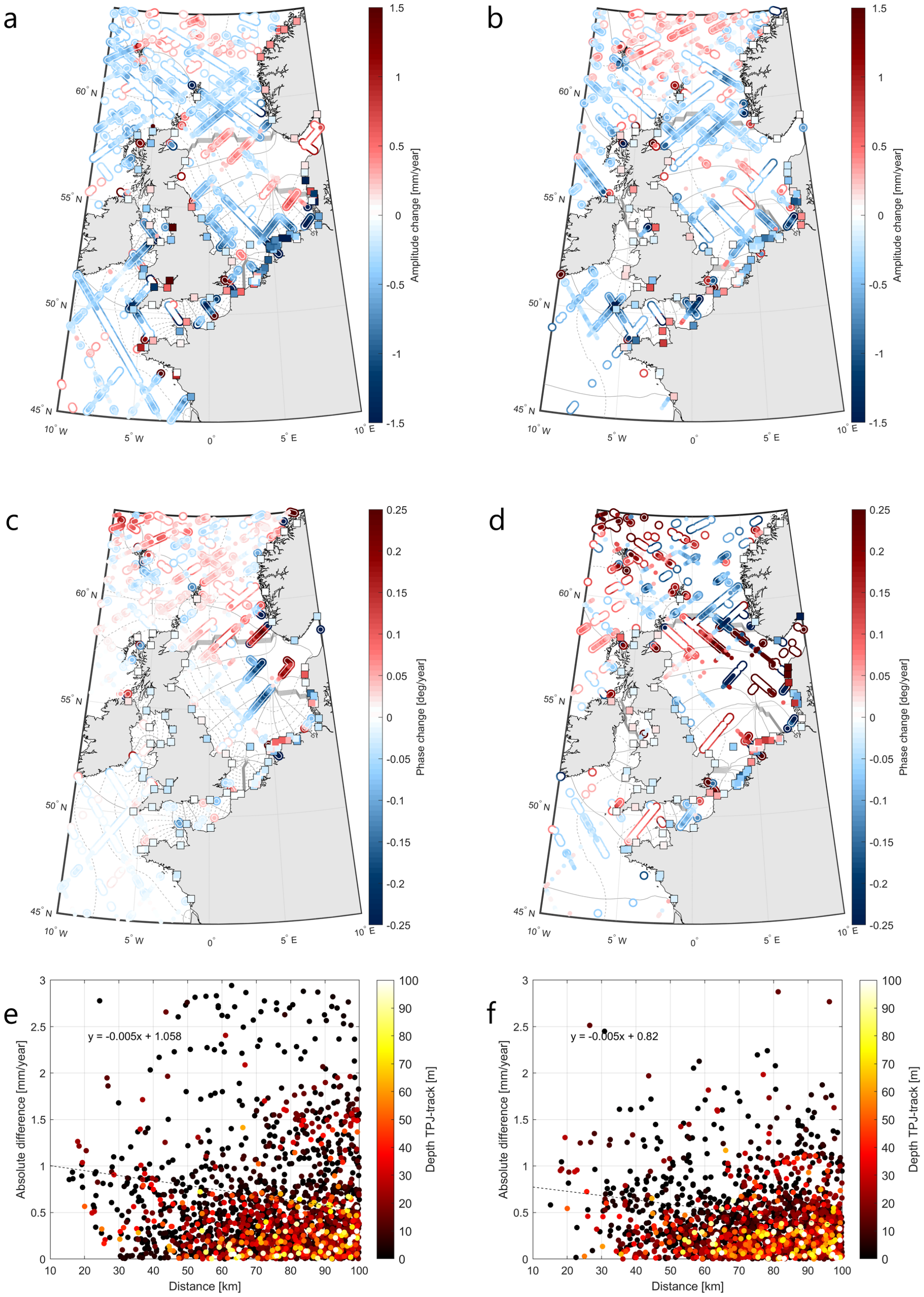

Figure 7: Linear change in M_2 amplitude (a), S_2 amplitude (b), M_2 phase (c) and S_2 phase (d) per year derived with the TintHA approach. The smaller solid scatters indicate significant trends given the UTide-derived confidence intervals, the hollow outline indicates significance according to the GTSM-derived confidence intervals (see Sect. 3 Methods). Co-tidal maps are shown in the background where the solid line indicates the phase at 45° intervals, the dashed lines show the amplitudes at 0.25 m intervals. Differences in amplitude change at TPJ-tracks compared to nearby tide gauges are shown in e (M_2) and f (S_2) as a function of distance and water depth at the TPJ-track.

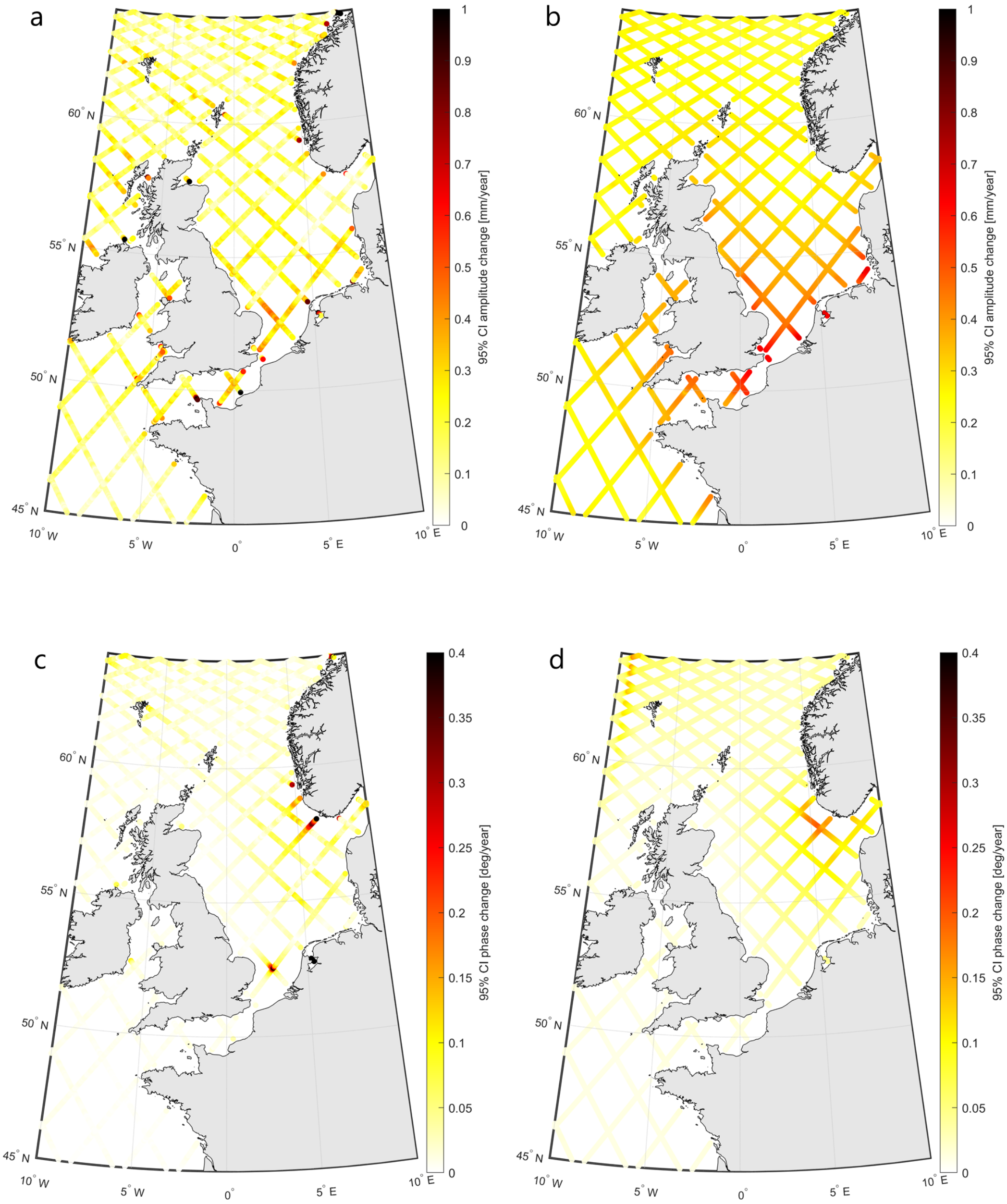

Figure 8: 95% confidence intervals for trend estimates derived from confidence intervals computed by UTide (a, c) and from standard errors derived from GTSM (b, d) for M_2 amplitudes (a, b) and M_2 phases (c, d).

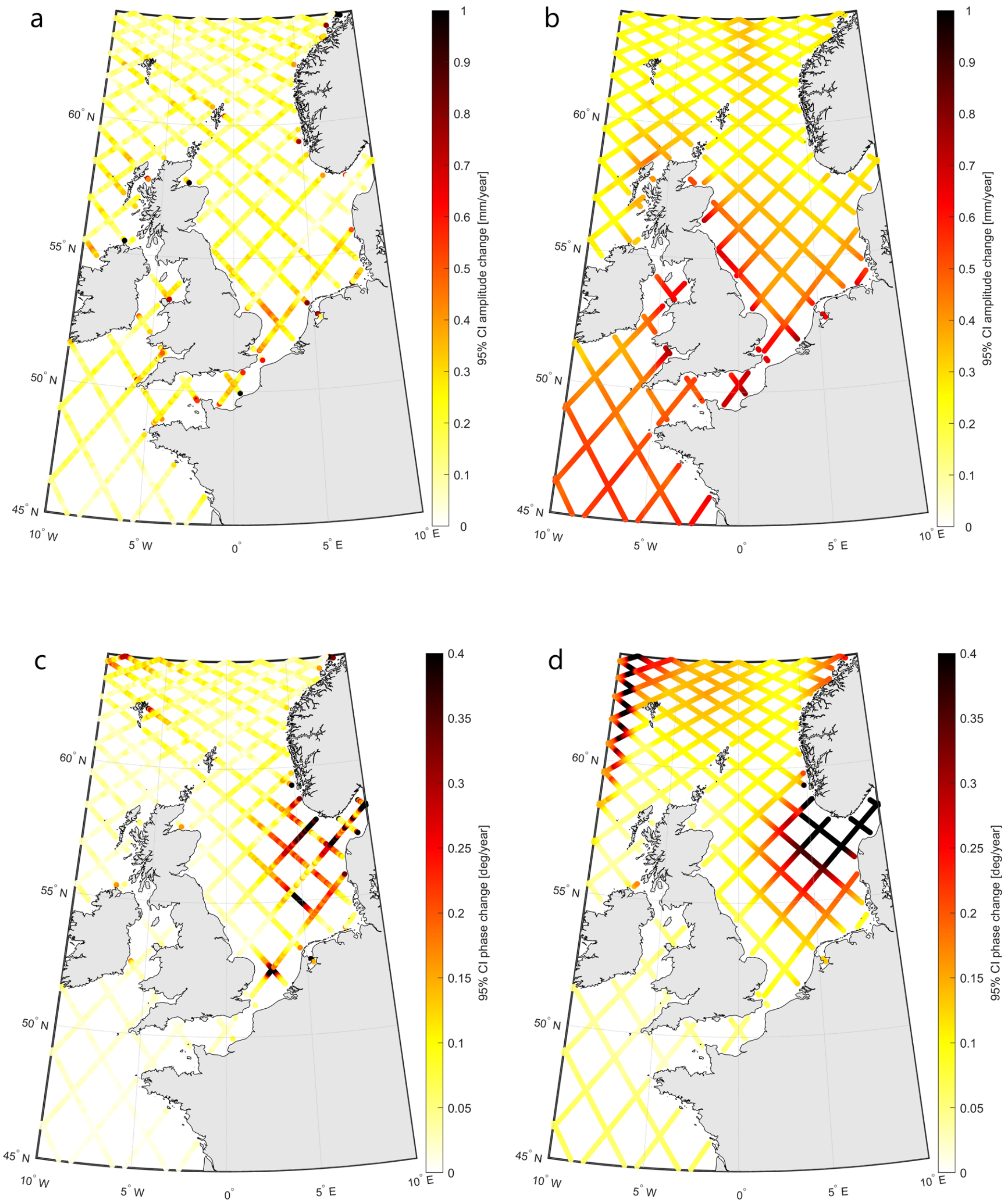

Figure 9: 95% confidence intervals for trend estimates derived from confidence intervals computed by UTide (a, c) and from standard errors derived from GTSM (b, d) for S_2 amplitudes (a, b) and S_2 phases (c, d).

harmonic constants was obtained. While satellite altimetry is routinely used for tidal analyses, this is the first time it was used to study secular trends on a global scale. Compared to tide gauges, the temporal resolution of the satellite data is limited. Consequently, several years of data were required to prevent aliasing and obtain reliable tidal estimates. Therefore, the method that is typically used to study secular changes in tides from tide gauge data, by means of yearly harmonic analysis, could not be applied. In this paper two alternative approaches were implemented. The first method (SegHA) is very similar to the yearly analysis except now the time series were divided into periods of four years. Compared to the yearly analysis, this reduces the number of consecutive independent tidal estimates and hence the redundancy in trend fitting and the significance of the estimated trends. Moreover, with this approach uncertainty estimates were obtained through a simplified error propagation whereby any correlation between the noise in amplitude and phases was ignored. However, this approach can be carried out with the standard available tidal software and allows a straightforward implementation of non-linear changes. On the other hand, in the second approach (TintHA) the linear change in tidal constants was estimated during the harmonic analysis. This way the entire time series could be analysed at once, which reduced the issue of aliasing. In the latter approach, no emperical correction for a possible residual of the nodal modulation was derived. However, results from the SegHA approach suggest this residual to be not significant on global scale (not shown here). Moreover, both methods produced very similar results, both when applied to the sub-sampled tide gauge data (Figure 1) and to the actual satellite radar altimeter data. Due to the rather low magnitudes of secular trends in tides (Figure 2, 3 and 7, S6 and S7), in many regions the magnitude of estimated trends just exceeds the uncertainty level (see Figures 4, 8, 9, S2 and S3).

The analysis described in this paper shows that it is possible to derive secular trends in tides from altimetry (TPJ in this case). However, caution is required. The results can strictly speaking not be validated since there is no comparable product available. The distance between tide gauges and the nearest TPJ-data exceeds $\sim$ 30 km in most cases and processes that affect tides near the coast may be very different from those at open sea. Moreover, the estimated trends at crossovers are spatial averages, that may not include all of the signal that is observed at tide gauges (being point estimates).

The main findings presented in this paper are as follows. The amplitudes of the considered tides have changed by up to 1 mm/year over the past $\sim$3 decades. This implies a change of up to 10 cm per century. The change in total tidal range remains unsure because many tidal constituents are not resolvable with the available data. Whether the amplitudes were subject to an increase or a decline varies on a regional (mainly applies to S_2) to even local basis (M_2, O_1, and K_1). On the North West European Shelf, relatively large phase changes are observed close to amphidromic points (Figure 7c, d) suggesting changes in amplitudes (Figure 7a, b) could be related to shifts of amphidromic points. However, from the experiment with tide gauge data it followed that the accuracy of derived phase changes reduces strongly when tidal amplitudes are low (Figure 1b, d), which is the case near amphidromic points. Possibly, the computed confidence intervals for these locations are too optimistic. This can be explained by the fact that the locations used for the GTSM confidence intervals do not coincide with the TPJ-tracks and/or location of amphidromic points.

For M_2, reasonable similarities were observed between secular trends derived from altimetry and at nearby tide gauges (Figure 7a, 7c). On the global scale, such comparisons may be deceptive given the distance between crossovers and the nearest tide gauge (Figure S1b) and significant spatial variability in change to the M_2 amplitude observed at tide gauges (Figure S1a). The magnitude and strong regional variability of the secular trends in M_2 amplitudes corresponds to findings by other studies based on tide gauge data (e.g., Müller et al., 2011; Schindelegger et al., 2018; Woodworth, 2010). However for S_2, O_1 and, K_1, more inconsistencies are observed between changes derived from altimetry and nearby tide gauges (Figure 7b, 7d). In addition, the altimeter-derived change in the S_2 tide differs from some documented findings (e.g., Ray, 2009; Woodworth, 2010). For instance, they found the S_2 amplitudes to have increased along the Gulf of Alaska. This contrasts both to what is derived from altimeter data at open ocean and our analysis of GESLA-3 tide gauge records (Figure 2b, 5b). This suggests that the difference may be related to the differences in considered periods. Moreover, such inconsistencies in S_2 may be associated with geophysical/range corrections applied to the TPJ-data, as any systematic error in the ionospheric, dry troposphere or atmospheric loading (DAC) correction could translate into a S_2-like signal (Zawadzki et al., 2018). For instance, the DAC was applied to TPJ-water levels to reduce the impact of aliasing of non-tidal water level variation on the estimation of tidal harmonic constants. For the sake of consistency, the same correction was applied to the tide gauge data, which is typically not done in earlier studies on tide gauge data. Therefore, a possible S_2-like signal in DAC (for instance related to the six-hour resolution of the product) may have affected the results. Moreover, errors in the model-derived ionospheric correction are found to leak into the solution of S_2 with an amplitude of up to several millimeters near the equator (e.g., Jee et al., 2010; Ray, 2020). This could potentially have affected our estimates of the linear change in this tide. However, no significant secular changes were observed in the S_2 amplitudes of this correction (not shown here) and the sensitivity of the linear change in S_2 to the source of the ionospheric correction was incorporated in the confidence intervals for this tide (Text S1). Finally, there may be intermission biases in range corrections that could be partly responsible for the observed trend in S_2 amplitudes, such as the CG-correction that was applied to TOPEX/Poseidon data (Beckley et al., 2021; Zawadzki et al., 2018). In general, the analysis of the S_2 is tricky and a more thorough analysis is deemed necessary.

The results presented in this paper merely allow speculation about the drivers behind the observed trends. The strong local variability in some areas suggests that local processes may dominate there or that the observed change is in fact related to internal tide variability. The internal M_2 tide has wavelengths of about ~ 160 km (Ray & Zaron, 2016). On the other hand, part of the observed signal could be related to sea ice decline (see e.g., Haigh et al., 2020). Namely, the observed changes in M_2 amplitude around Iceland (Figure 2a) are of opposite sign compared to the March-September amplitude differences documented by Bij de Vaate et al. (2021). This indicates that over time the annual average tide becomes closer to the September case, which is in line with interannual sea ice decline. This may also explain the increased spatial correlation in observed trends in M_2 amplitudes near the poles. Furthermore, changes in tides have been linked to sea level rise. For instance, the modelled effect of SLR on M_2 amplitudes was found to be ~ 10 cm/m SLR (e.g., Pickering et al., 2017; Schindelegger et al., 2018). This, given a SLR of ~ 3 mm/year since 1990, is of comparable magnitude to the TPJ-derived amplitude changes in most regions (~ 0.3 mm/year). However, the modelled M_2 amplitude change under the influence of SLR does not exhibit the large regional variability that was seen in the altimetry-derived trends, although a number of similarities can be observed on for instance the North West European Shelf. On another note, the zonal pattern in the S_2 amplitude change is striking and not present for the other (lunar) tides. If the observed change is in fact related to the tide and not to other non-tidal processes, this suggests the causes to be related to radiational forcing. About 15% of the S_2 tide is driven by pressure loading of the ocean (Haigh et al., 2020) and interannual variability in atmospheric pressure could translate into variable S_2 amplitudes. Given that atmospheric pressure fluctuates continuously (Lu & Tu, 2021), it may be that the secular change in S_2 amplitude cannot be accurately described by a linear trend.

With this study we have demonstrated the possibilities provided by satellite altimetry in deriving secular trends in global tides. The use of satellite altimetry for this purpose clearly increases the spatial data coverage, yet introduces other issues related to its low data availability in temporal sense. To overcome these issues, two alternative approaches were implemented that produced reasonably similar results. On another note, the presented study considers both trend uncertainties derived from UTide and from modeled time series. From a comparison of both products (e.g. Figure 8 and 9) it appears that the uncertainties obtained by UTide are indeed reasonable, that is, they are of similar order of magnitude as the GTSM-derived uncertainties. However, in particular in shelf regions, the uncertainties are most likely underestimated by UTide. Here one would expect larger uncertainties due to larger non-tidal residuals and unresolved shallow water tides, while the UTide-derived uncertainties are equally low and homogeneous in shelf regions as on the open ocean. Likely, the application of the 'mesoscale correction' in shallow water removes some tidal signal that is aliased in the SLA product that was used for this correction (Zaron & Ray, 2018). This would reduce the residuals and hence it may have caused too optimistic uncertainty estimates by UTide. In this respect, the GTSM-derived method may have obtained more reasonable uncertainty estimates, indicating the added value of this product. Nevertheless, the GTSM-derived uncertainties could for instance not explain all ambiguities at crossing tracks (Figure 7a-d). For future studies, we recommend the use of a full 3D model that allows for direct comparison of the data and model time series. Such a model would include the mesoscale variability that is also present in the satellite radar altimeter data and allow for the same corrections to be applied to both the actual data and model time series. Furthermore, the analysis could possibly benefit from the addition of data from other satellite missions. However, given the low magnitude of the observed secular trends, even small intermission biases in the range corrections could be easily mistaken for changes in the actual tides. Finally, although we can at this stage not draw conclusions on the drivers behind the observed changes in tides, our findings could be useful for future (modelling) studies on this phenomenon.

Acknowledgments

This work is part of the research programme FAST4Nl with project number ALWPP.2017.001, which is (partly) financed by the Dutch Research Council (NWO). Tide gauge data were kindly provided by the Agentschap Maritieme Dienstverlening en Kust, Belgium; Danish Coastal Authority; Danish Meteorological Institute; Danish Maritime Safety Administration; Service Hydrographique et Océanographique de la Marine, France; Die Wasserstraßen- und Schifffahrtsverwaltung des Bundes, Germany; Rijkswaterstaat, Netherlands; Norwegian Hydrographic Service, and U.K. National Tidal and Sea Level Facility (NTSLF). The reanalysis data (GTSM) were kindly provided by Deltares, Netherlands. The GESLA-3 data set was obtained from `https://www.icloud.com/iclouddrive/0tHXOLCgBBjgmpHecFsfBXLag#GESLA3`, the DUACS SLA product from `https://doi.org/10.48670/moi-00148` and the RADS data can be accessed through `http://rads.tudelft.nl/rads/rads.shtml`. The estimated secular trends from TPJ-data are made available here: `https://doi.org/10.4121/17086394`

References

Beckley, B., Ray, R. D., Zelensky, N., Lemoine, F., Brown, S., Desai, S., & Mitchum, G. (2021). Integrated Multi-Mission Ocean Altimeter Data for Climate Research TOPEX/Poseidon, Jason-1, 2, 3 User's Handbook Version 5.1.

Bij de Vaate, I., Vasulkar, A. N., Slobbe, D. C., & Verlaan, M. (2021). The Influence of Arctic Landfast Ice on Seasonal Modulation of the M2 Tide. *Journal of Geophysical Research: Oceans*, *126*, e2020JC016630.

Cartwright, D. E., & Edden, A. C. (1973). Corrected tables of tidal harmonics. *Geophys. J. Roy. Astron. Soc.*, *33*, 253–264. doi: doi:10.1111/j.1365-246X.1973.tb03420.x

Cartwright, D. E., & Taylor, R. J. (1971). New computations of the tide-generating potential. *Geophys. J. Roy. Astron. Soc.*, *23*, 45–74. doi: doi:10.1111/j.1365-246X.1971.tb01803.x

Cherniawsky, J. Y., Foreman, M. G., Kang, S. K., Scharroo, R., & Eert, A. J. (2010). 18.6-year lunar nodal tides from altimeter data. *Continental Shelf Research*, *30*(6), 575–587.

Codiga, D. L. (2011). *Unified Tidal Analysis and Prediction Using the UTide Matlab Functions. Technical Report 2011-01.* Graduate School of Oceanography, University of Rhode Island: Narragansett.

Codiga, D. L. (2020). *UTide Unified Tidal Analysis and Prediction Functions. MATLAB Central File Exchange.* https://www.mathworks.com/matlabcentral/fileexchange/46523-utide-unified-tidal-analysis-and-prediction-functions. (Last checked on 10/06/2020)

Dangendorf, S., Calafat, F. M., Arns, A., Wahl, T., Haigh, I. D., & Jensen, J. (2014). Mean sea level variability in the North Sea: Processes and implications. *Journal of Geophysical Research: Oceans*, *119*(10).

Devlin, A. T., Jay, D. A., Talke, S. A., Zaron, E. D., Pan, J., & Lin, H. (2017). Coupling of sea level and tidal range changes, with implications for future water levels. *Scientific Reports*, *7*(1), 1-–12.

Foreman, M. G. G. (2004). *Manual for tidal heights analysis and prediction, revised.* Pacific Marine Science Rep. 77, 10.

Guarneri, H., Verlaan, M., Slobbe, D. C., Veenstra, J., & F., Z. (2022). Estimating tides from satellite radar altimetry in coastal seas. *Marine Geodesy*, *XX*, XX–XX. (Manuscript in preparation)

Hagen, R., Plüß, A., Jänicke, L., Freund, J., Jensen, J., & Kösters, F. (2021). A combined modeling and measurement approach to assess the nodal tide modulation in the North Sea. *Journal of Geophysical Research: Oceans*, *126*, e2020JC016364.

Haigh, I. D., Marcos, M., Talke, S. A., Woodworth, P. L., Hunter, J. R., Haugh, B. S., ... Thompson, P. (2021). GESLA Version 3: A major update to the global higher-frequency sea-level dataset. *EarthArXiv*. doi: https://doi.org/10.31223/X5MP65

Haigh, I. D., Pickering, M. D., Green, J. M., Arbic, B. K., Arns, A., Dangendorf, S., ... Woodworth, P. L. (2020). The tides they are a-Changin': A comprehensive review of past and future nonastronomical changes in tides, their driving mechanisms, and future implications. *Reviews of Geophysics*, *58*(1), e2018RG000636.

Hinton, A. C. (2000). Tidal changes and coastal hazards: past, present and future. *Natural Hazards*, *21*(2), 173–184.

Jee, G., Lee, H. B., Kim, Y. H., Chung, J. K., & Cho, J. (2010). Assessment of GPS global ionosphere maps (GIM) by comparison between CODE GIM and TOPEX/Jason TEC data: Ionospheric perspective. *Journal of Geophysical Research: Space Physics*, *115*(A10).

Jin, G., Pan, H., Zhang, Q., Lv, X., Zhao, W., & Gao, Y. (2018). Determination of harmonic parameters with temporal variations: An enhanced harmonic analysis algorithm and application to internal tidal currents in the South China Sea. *Journal of atmospheric and oceanic technology*, *35*(7), 1375-–1398.

Khojasteh, D., Glamore, W., Heimhuber, V., & Felder, S. (2021). Sea level rise impacts on estuarine dynamics: A review. *Science of The Total Environment*, 146470.

Li, S., Wahl, T., Talke, S. A., Jay, D. A., Orton, P. M., Liang, X., ... Liu, L. (2021). Evolving tides aggravate nuisance flooding along the US coastline. *Science Advances*, *7*(10), eabe2412.

Lu, E., & Tu, J. (2021). Relative importance of surface air temperature and density to interannual variations in monthly surface atmospheric pressure. *International Journal of Climatology*, *41*, E819–E831.

Müller, M. (2012). The influence of changing stratification conditions on barotropic tidal transport and its implications for seasonal and secular changes of tides. *Continental Shelf Research*, *47*, 107–118. doi: https://doi.org/10.1016/j.csr.2012.07.003

Müller, M., Arbic, B. K., & Mitrovica, J. X. (2011). Secular trends in ocean tides: Observations and model results. *Journal of Geophysical Research: Oceans*, *116*(C5).

Müller, M., Cherniawsky, J. Y., Foreman, M. G. G., & von Storch, J. S. (2014). Seasonal variation of the M 2 tide. *Ocean Dynamics*, *64*(2), 159–177. doi: https://doi.org/10.1007/s10236-013-0679-0

Pawlowicz, R., Beardsley, B., & Lentz, S. (2002). Classical tidal harmonic analysis including error estimates in MATLAB using T-TIDE. *Computers & Geosciences*, *28*, 929-937.

Pickering, M. D., Horsburgh, K. J., Blundell, J. R., Hirschi, J. M., Nicholls, R. J., Verlaan, M., & Wells, N. C. (2017). The impact of future sea-level rise on global tides. *Continental Shelf Research*, *142*, 50–68.

Ray, R. D. (2009). Secular changes in the solar semidiurnal tide of the western North Atlantic Ocean. *Geophysical Research Letters*, *36*(29), 108–116.

Ray, R. D. (2016). On measurements of the tide at Churchill, Hudson Bay. *Atmosphere-Ocean*, *54*(2), 108–116.

Ray, R. D. (2020). Daily harmonics of ionospheric total electron content from satellite altimetry. *Journal of Atmospheric and Solar-Terrestrial Physics*, *209*, 105423.

Ray, R. D., & Zaron, E. D. (2016). M_2 Internal Tides and Their Observed Wavenumber Spectra from Satellite Altimetry. *Journal of Physical Oceanography*, *46*(1), 3–22.

Ross, A. C., Najar, R. G., Li, M., Lee, S. B., Zhang, F., & Liu, W. (2017). Fingerprints of sea level rise on changing tides in the Chesapeake and Delaware Bays. *Journal of Geophysical Research: Oceans*, *122*, 8102–8125. doi: doi:10.1002/2017JC012887

Savcenko, R., & Bosch, W. (2007). Residual Tide Analysis in Shallow Water-Contributions of ENVISAT and ERS Altimetry. *ESA-SP636 (CD-ROM), Proceedings of the Envisat Symposium*.

Scharroo, R., Leuliette, E. W., Naeije, M. C., Martin-Puig, C., & Pires, N. (2016). RADS Version 4: An efficient way to analyse the multi-mission altimeter database. *Proceedings of the ESA Living Planet Symposium*, 9–13. (ESA Special Publication SP-740)

Schindelegger, J. A. M., M. Green, Wilmes, S. B., & Haigh, I. D. (2018). Can we model the effect of observed sea level rise on tides? *Journal of Geophysical Research: Oceans*, *123*, 4593–4609.

Schrama, E. J. O., & Ray, R. D. (1994). A preliminary tidal analysis of TOPEX/POSEIDON altimetry. *Journal of Geophysical Research: Oceans*, *99*(C12), 24799–24808.

St-Laurent, P., Saucier, F. J., & Dumais, J. F. (2008). On the modification of tides in a seasonally ice-covered sea. *Journal of Geophysical Research: Oceans*, *113*(11), 1–11. doi: https://doi.org/10.1029/2007JC004614

Taburet, G., Sanchez-Roman, A., Ballarotta, M., Pujol, M. I., Legeais, J. F., Fournier, F., … Dibarboure, G. (2019). DUACS DT2018: 25 years of reprocessed sea level altimetry products. *Ocean Science*, *15*(5), 1207-–1224.

Wahr, J. M. (1985). Deformation induced by polar motion. *Journal of Geophysical Research*, *90*(B11), 9363–9368. doi: doi:10.1029/JB090iB11p09363

Wang, X., Verlaan, M., Apecechea, M. I., & Lin, H. X. (2021). Computation-efficient Parameter Estimation for a High-Resolution Global Tide and Surge Model (GTSM). *Journal of Geophysical Research: Oceans*, *126*, e2020JC016917. doi: https://doi.org/10.1029/2020JC016917

Woodworth, P. L. (2010). A survey of recent changes in the main components of the ocean tide. *Continental shelf research*, *30*(15), 1680–1691.

Zaron, E. D., & Ray, R. D. (2018). Aliased Tidal Variability in Mesoscale Sea Level Anomaly Maps. *Journal of Atmospheric and Oceanic Technology*, *35*(12), 2421—2435.

Zawadzki, L., Ablain, M., Carrere, L., Ray, R. D., Zelensky, N. P., Lyard, F., … Picot, N. (2018). Investigating the 59-Day Error Signal in the Mean Sea Level

Derived From TOPEX/Poseidon, Jason-1, and Jason-2 Data With FES and GOT Ocean Tide Models. *IEEE TRANSACTIONS ON GEOSCIENCE AND REMOTE SENSING*, *56*(6), 3244–3255.

References From the Supporting Information

Fernandes, M. J., Lázaro, C., Nunes, A. L., Scharroo, R. (2014). Atmospheric corrections for altimetry studies over inland water. Remote Sensing, 6(6), 4952-4997.